Hyperfine Interact (2019) 240: 25
https://doi.org/10.1007/s10751-019-1568-9

Local structure study of ^{181}Hf dopants in Zr_7Ni_{10} by perturbed angular correlation spectroscopy and first principles calculations

Sourav Kumar Dey[1,2] · Chandi Charan Dey[1,2] · Satyajit Saha[1,2] · Debashis Banerjee[2,3] · Dragan Toprek[4]

Published online: 19 March 2019

Abstract

Intermetallic compound Zr_7Ni_{10} has been studied by perturbed angular correlation (PAC) spectroscopy to determine the electric field gradient and site occupation of Hf dopant in the compound. A mixture of phase components were found in this sample. The component with $V_{zz} = 6.6(1)\times10^{21}$ V/m^2 and $\eta = 0.71(1)$ at room temperature has been assigned to Zr_7Ni_{10} phase. In this sample, Zr_2Ni_7 and Zr_8Ni_{21} phases were also found to be present along with Zr_7Ni_{10}. No phase transition is observed in the temperature range 77-1073 K in this sample. The electric field gradient (V_{zz}) for Zr_7Ni_{10} phase was found to decrease linearly with temperature. The phase components in Zr_7Ni_{10} have been determined also from X-ray powder diffraction (XRD) measurement. Theoretical calculations of EFG have been performed in Ta-doped Zr_7Ni_{10} using all electron full potential (linearized) augmented plane wave [FP-(L)APW] method, within the framework of the density functional theory (DFT) to compare the results with the values obtained from PAC measurements and to know the site preference of ^{181}Ta probe in the host matrix.

Keywords Zr_7Ni_{10} intermetallic alloy · Perturbed angular correlation spectroscopy · X-ray diffraction · ab initio calculations

This article has been corrected because one of the authors given names was incorrect.

This article is part of the Topical Collection on *Proceedings of the International Conference on Hyperfine Interactions and their Applications (HYPERFINE 2019), Goa, India, 10-15 February 2019*
Edited by S. N. Mishra, P. L. Paulose and R. Palit

✉ Sourav Kumar Dey
skumar.dey@saha.ac.in

[1] Applied Nuclear Physics Division, Saha Institute of Nuclear Physics, 1/AF Bidhannagar, Kolkata 700 064, India

[2] Homi Bhabha National Institute, Anushaktinagar, Mumbai 400 094, India

[3] Accelerator Chemistry Section, RCD (BARC), Variable Energy Cyclotron Centre, Kolkata 700064, India

[4] Institute of Nuclear Sciences Vinca, University of Belgrade, P. O. Box 522, 11001 Belgrade, Serbia

1 Introduction

The alloys based on Zr-Ni system have numerous technological applications. Some of the Zr-Ni binary alloys, viz. Zr_8Ni_{21}, Zr_7Ni_{10}, ZrNi and Zr_9Ni_{11} [1–7] have received considerable attention due to their ability to absorb large amount of gaseous hydrogen and reversibility in hydrogen dissociation process. These alloys form metal hydrides (MH) after hydrogen absorption and these MHs are used as negative electrodes in Ni-MH rechargeable batteries. The Ni-MH batteries have been widely used in hybrid electric vehicles (HEV) due to their high energy density. Electrochemical capacity is found to be maximum for Zr_7Ni_{10} among Zr-Ni binary alloys [5].

The crystal structure of Zr_7Ni_{10} was first reported to be a non-centrosymmetric orthorhombic structure with space group $Aba2$ by Kirkpatrick et al. [8]. Later on, Joubert et al. [9] corrected the crystal structure to be centrosymmetric orthorhombic structure with space group $Cmca$.

The perturbed angular correlation is a useful nuclear technique to study the structural properties, phase transitions, crystalline defects and magnetic ordering in intermetallic compounds [10]. Recently we have studied two Zr-Ni compounds which have hydrogen storage properties. These are Zr_8Ni_{21} [11], Zr_9Ni_{11} [12]. In the present report, studies in another hydrogen absorbing material Zr_7Ni_{10} have been carried out by PAC to determine the electric field gradient (EFG) at the ^{181}Ta probe impurity site in the material. To the best of our knowledge, no previous investigation in Zr_7Ni_{10} was done by PAC spectroscopy. Theoretical calculations of EFG at Ta doped Zr_7Ni_{10} matrix have been done to compare the results with the measured values from PAC spectroscopy and to determine the site preference of ^{181}Ta probe atom in the host lattice Zr_7Ni_{10}. Temperature dependent PAC measurements in Zr_7Ni_{10} have been carried out to determine the phase components produced in the sample and their stabilities with temperature in the range 77-1073 K.

2 Experimental details

We have prepared the Zr_7Ni_{10} sample by arc melting of high purity Zr and Ni metals taken in stoichiometric ratio in argon atmosphere. These metals were procured from Alfa Aesar. The purity of Zr was $\sim$ 99.2% excluding Hf (maximum Hf concentration 4.5 wt%). The purity of Ni used was 99.98%. The sample was remelted with a tiny piece (<1 at%) of natural Hf metal wire which was then activated to ^{181}Hf by irradiating with thermal neutrons using a flux of $\sim 10^{13}$/cm^2/s at Dhruba reactor, Mumbai, for seven days. Inactive sample of Zr_7Ni_{10} was prepared separately in the argon arc furnace in a similar manner for XRD measurement. The XRD measurement was carried out by TTRAX-III X-ray diffractometer (Rigaku, Japan) using the Cu K_α radiation.

PAC measurements with ^{181}Hf(β^-)^{181}Ta probe were performed using a four detector $LaBr_3$(Ce)-BaF_2 set up. A typical time resolution of 790 ps was found at 131-482 keV γ-ray energy selection using a prompt source (^{22}Na). Four slow-fast coincidence combinations were built to collect data at 180° and 90°. The conventional ratio of coincident count rate is obtained from the following relation

$$R(t) = \frac{2}{3}\left[\sqrt{\frac{N_{13}(180^\circ, t)N_{24}(180^\circ, t)}{N_{14}(90^\circ, t)N_{23}(90^\circ, t)}} - 1\right], \quad (1)$$

where $N_{ij}(\theta, t)$ (θ: angle between the detectors) is the background subtracted coincident count rate at time channel t. To form this ratio, the time zero channel for each spectrum

was measured using a prompt source and time calibration for the spectrum was accurately determined by using a time calibrator (ORTEC 462). To analyze the PAC spectrum for spin $I = 5/2\ \hbar$ of the intermediate energy level of ^{181}Ta probe in a polycrystalline sample, we have used the following expression of the perturbation factor [10, 13, 14],

$$G_2(t) = S_{20}(\eta) + \sum_{n=1}^{3} S_{2n}(\eta)\cos(\omega_n t)\exp(-\delta\omega_n t). \quad (2)$$

The ratio $R(t)$ is related to the perturbation factor by the relation $A_2 G_2(t) = \frac{R(t)}{1+R(t)/2}$ (angular correlation coefficient A_2 for 133-482 keV cascade of ^{181}Ta = -0.288). Because $A_2 \gg A_4$ for this cascade, only A_2 is considered. The ω_n are the transition frequencies between the three sublevels of the intermediate level arising due to hyperfine splitting. The S_{2n} (n=0,1,2,3) parameters depend on the asymmetry of the electric field gradient (EFG) and these are expressed as a polynomial in asymmetry parameter (η). Due to lattice strain or defects present in a real crystal, different probes are subjected to slightly different electronic and ionic environment in the same phase of the crystal. This effect is considered by an exponential (Lorntzian) distribution function where δ is mean frequency distribution width. Transition frequencies ω_i are obtained by least squares fitting of the experimental PAC data with the (2) which are then used to determine quadrupole frequency ω_Q. For each measured ω_Q, the electric field gradient (V_{zz}) is obtained from the relation $\omega_Q = \frac{eQV_{zz}}{4I(2I-1)\hbar}$. Now, if the probe nuclei are exposed to a different crystal environment in a sample, the perturbation functions will be different for each of these sites and the total perturbation function is obtained taking sum over all the different perturbation functions: $G_2(t) = \sum_i f_i G_2^i(t)$, where f_i is the fraction of atoms in the ith site and $G_2^i(t)$ is the corresponding perturbation function. The asymmetry parameter η is defined as $\eta = \frac{V_{xx}-V_{yy}}{V_{zz}}$.

3 Results and discussion

3.1 Zr_7Ni_{10}

The XRD powder pattern obtained in stoichiometric Zr_7Ni_{10} sample is shown in Fig. 1. Peaks were first identified using ICDD database. The presence of orthorhombic Zr_7Ni_{10} ([9], PDF Card No.: 01-072-3501), triclinic Zr_8Ni_{21} ([15], PDF Card No.: 01-071-2622) and monoclinic Zr_2Ni_7 ([16], PDF Card No.: 01-071-0543) phases have been found from XRD analysis. The X-ray intensity profile has been fitted using FULLPROF software package [17].

The PAC spectrum in the stoichiometric Zr_7Ni_{10} sample at room temperature is shown in Fig. 2. The spectrum is found to be best fitted by considering five quadrupole frequencies. Texture effects are observed in the sample. Therefore, the spectrum is analyzed using free S_{2n} (n=0,1,2,3) parameters. At room temperature, a major component ($\sim$ 38%) is found with values of ω_Q = 72.7(3) Mrad/s, η = 0.12(4) and δ = 1.1(7)%. This component can be assigned to Zr_2Ni_7 by comparing with the results found in Zr_2Ni_7 [18]. The second major component ($\sim$25%) with values of ω_Q = 58.9(3) Mrad/s, η = 0.71(1) is attributed to Zr_7Ni_{10} phase by comparing the result with our DFT calculation (discussed later). A minor component ($\sim$11%) was found to be present with values of ω_Q = 77.1(9) Mrad/s, η = 0.81(2) which has been identified as Zr_8Ni_{21} by comparing the result with our recent PAC investigation in Zr_8Ni_{21} [11]. Apart from these components, two other

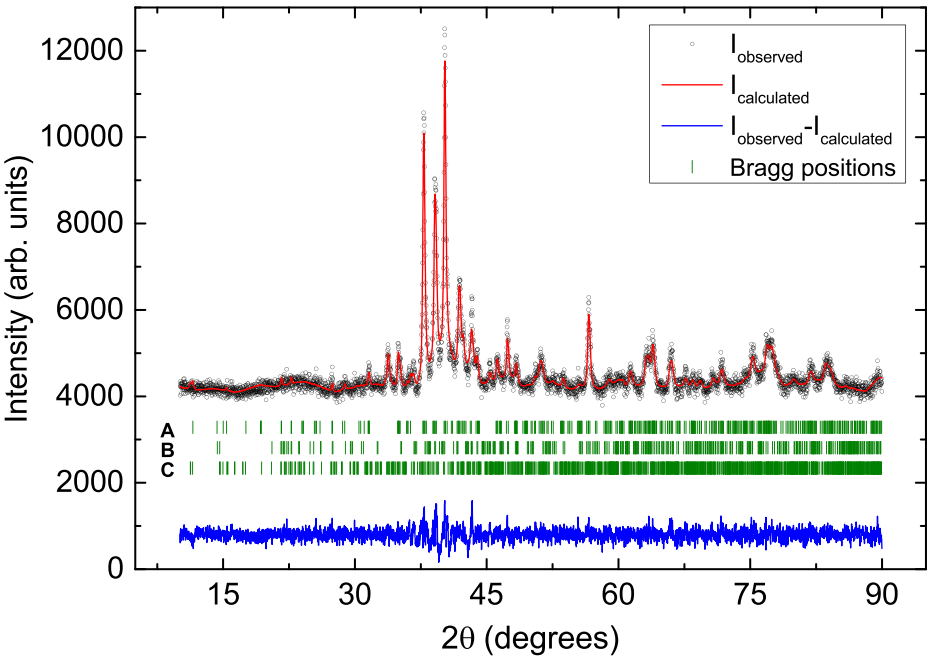

Fig. 1 The background subtracted XRD powder pattern in the stoichiometric sample of Zr_7Ni_{10}. The vertical bars A, B and C denote the Bragg angles corresponding to Zr_7Ni_{10}, Zr_2Ni_7 and Zr_8Ni_{21} phases, respectively

minor frequency components (ω_Q=8.0(7) Mrad/s, η=0, f=17%; ω_Q=33(1) Mrad/s, η=0, f=9%) have been found. These two components are attributed to defects. Since the activation of the sample was done after preparing the sample, crystalline defects can be produced during neutron irradiation [19] of the sample. From the Zr-Ni phase diagram, it is found that the phase Zr_2Ni_7 melts congruently and Zr_8Ni_{21} phase is formed peritectically from Zr_2Ni_7 and liquid melt ($L+Zr_2Ni_7 \rightarrow Zr_8Ni_{21}$) at 1453 K [20]. The phases Zr_7Ni_{10} and Zr_8Ni_{21} are formed from liquid alloy by an eutectic reaction ($L \rightarrow Zr_8Ni_{21}+Zr_7Ni_{10}$) [20] at 1333 K.

At 77 K, the Zr_2Ni_7 and Zr_7Ni_{10} phases were found only. All the three Zr-Ni phases, viz. Zr_2Ni_7, Zr_8Ni_{21} and Zr_7Ni_{10} are present in the temperature range 298-773 K. At 873 K and above, the component due to Zr_8Ni_{21} does not appear (Fig. 2). The phases Zr_2Ni_7 and Zr_7Ni_{10}, however, remain stable up to 1073 K. The phase Zr_2Ni_7 is found to be predominant in the whole temperature range (77-1073 K) among the Zr-Ni binary phases that are produced in Zr_7Ni_{10} sample. The frequency values for the fourth and fifth components show anomalous temperature dependence. This further indicates that these are irregular defect components. A re-measurement is carried at room temperature after measurement at 1073 K. Here, all the three Zr-Ni phases, viz. Zr_2Ni_7, Zr_7Ni_{10} and Zr_8Ni_{21} were produced reversibly with almost same fractions.

Temperature evolution of quadrupole frequency and asymmetry parameter for two Zr-Ni phases, viz. Zr_2Ni_7 and Zr_7Ni_{10} present in the Zr_7Ni_{10} sample are shown in Fig. 3. The asymmetry parameter of Zr_7Ni_{10} phase increases with temperature. The quadrupole frequencies for both the components decrease linearly with temperature. The values of

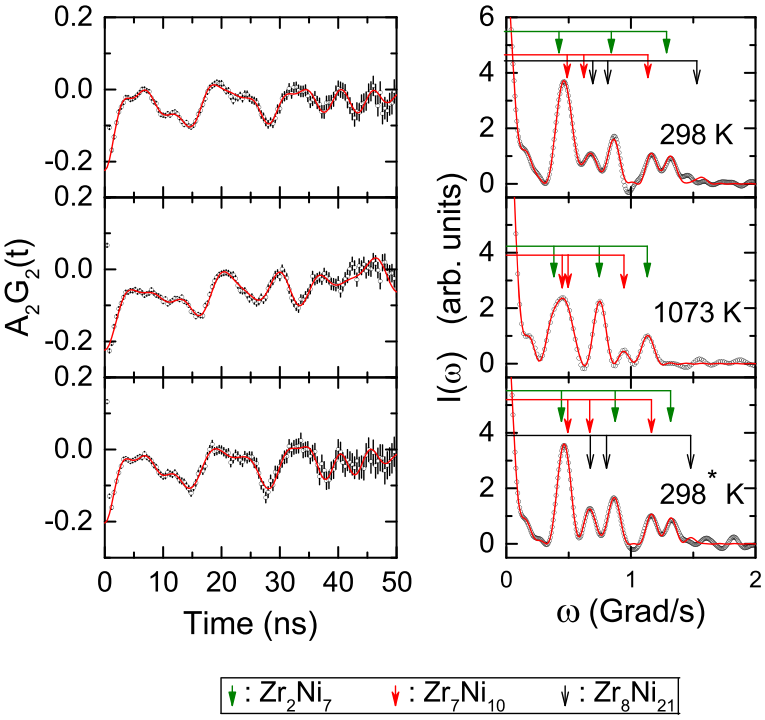

Fig. 2 Perturbed angular correlation spectra in Zr_7Ni_{10} at different temperatures. Left panel shows the time spectra and the right panel shows the corresponding Fourier cosine transforms. The PAC spectrum designated by 298* K is taken at room temperature after the measurement at 1073 K

quadrupole frequencies obtained for Zr_2Ni_7 and Zr_7Ni_{10} phases in the temperature range 77-1073 K have been fitted with the following relation

$$\omega_Q(T) = \omega_Q(0)[1 - \alpha T]. \tag{3}$$

The fitted results give $\omega_Q(0)$ = 65(1) Mrad/s (V_{zz} = 7.3(2)×10^{21} V/m^2), α = 3.1(3)×10^{-4} K^{-1} for Zr_7Ni_{10} component. For the Zr_2Ni_7 component, the results are $\omega_Q(0)$ = 77(1) Mrad/s (V_{zz} = 8.6(2)×10^{21} V/m^2), α = 2.1(2)×10^{-4} K^{-1}. The linear temperature dependence of quadrupole frequency was observed in many intermetallic compounds [21–27].

4 DFT calculations and results

Zr_7Ni_{10} crystallizes in the orthorhombic base-centered centrosymmetric *Cmca* type structure (space group number 64) with lattice parameters *a*=12.381 Å, *b*=9.185 Å and *c*=9.221 Å [9]. This structure contains 34 atoms in the unit cell and possesses 7 non-equivalent crystallographic positions; 4 non-equivalent positions for Zr and 3 non-equivalent positions for Ni.

First we have optimized these structural parameters. The first-principles density functional theory (DFT) calculations were performed to compare with the experimental results. All the calculations were done using the full potential (linearized) augmented plane waves method [FP-(L)APW], as implemented in WIEN2k [28]. The energy convergence has been

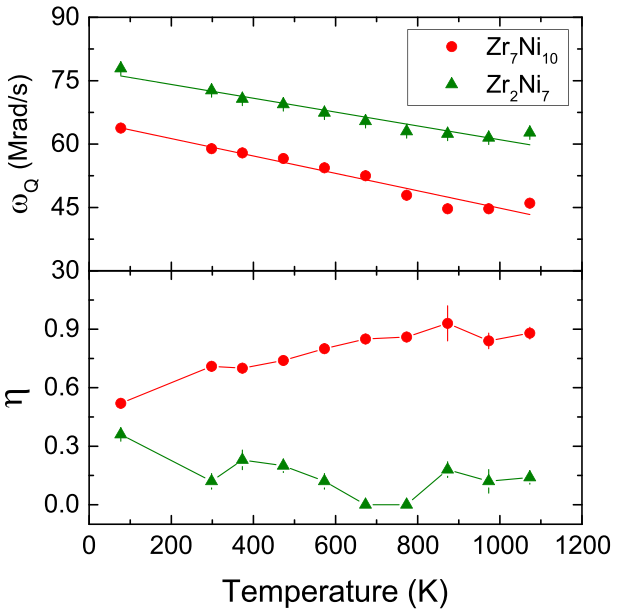

Fig. 3 Variations of quadrupole frequency (ω_Q) and asymmetry parameter (η) with temperature for the components of Zr_7Ni_{10} and Zr_2Ni_7

achieved by expanding the basis function up to $R_{MT} \cdot K_{max}$=7, where R_{MT} is the smallest atomic sphere radius in the unit cell and K_{max} gives the magnitude of the largest $\vec{k}$ vector in the plane wave expansion. In our calculations the muffin-tin radii for Zr, Ni and Ta were 2.2, 2.1 and 2.15 a. u., respectively. The valence wave functions inside the spheres are expanded up to l_{max}=10 while the charge density is Fourier expanded up to G_{max}=16. The energy to separate core and valence states was set to -7 Ry. Electronic exchange-correlation energy was treated with generalized gradient approximation (GGA) parametrized by Perdew-Burke-Ernzerhof (PBE) [29–31]. Taking into consideration both the accuracy and the efficiency of the calculations, we have selected a 8×8×8 k point mesh to sample the entire Brillouin-zone (BZ), yielding 143 points in the irreducible Brillouin-zone. The structure was relaxed according to Hellmann-Feynman forces calculated at the end of each self-consistent cycle, until the forces acting on all atoms were less than 0.068 eV/Å (5 mRy/a.u.). The relaxation method is described in Ref. [32]. In our calculations the self-consistency was achieved by demanding the convergence of the integrated charge difference between last two iterations to be smaller than 10^{-5}e. All the calculations refer to zero temperature.

After obtaining the optimized structural parameters, we replaced one of the host sites; i.e. one of the 4 non-equivalent positions of Zr by a Ta atom (preserving the point group symmetry around original atom), in order to simulate a dopant in the crystal lattice. This substitutional structures have been marked as Zr1-Ta, Zr2-Ta, Zr3-Ta and Zr4-Ta. For each case of the substitutional structure, we have repeated calculations again, keeping all parameters and charge convergence criteria same as in the case of the pure compounds. For example, to simulate PAC measurements at Zr1 position, we replaced one atom at position (0, 0.31359, 0.18707) with Ta atom. We checked that the two Ta atoms are sufficiently far from each

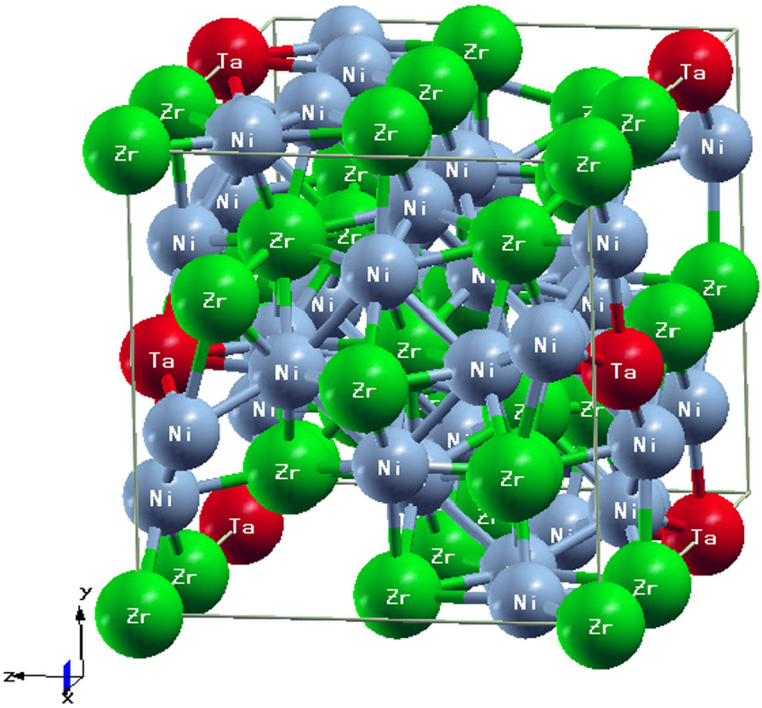

Fig. 4 Model of cell used in the study of Zr_7Ni_{10} by replacing Zr3 atom with Ta probe

other (∼8 Å) to avoid significant impurity-impurity interactions. The sign of EFG (V_{zz}) can not be determined from PAC measurement. Thus, absolute values of measured EFG (extrapolated to 0 K) and asymmetry parameter (at 77 K) for Zr_7Ni_{10} have been compared with the theoretical results. The calculation of EFG were performed by using the method developed in Ref. [33] which is implemented in WIEN2k code. All the calculations refer to zero temperature.

We see that the calculated result for EFG at the Ta probe site replacing Zr3 atom (Fig. 4; 6.99×10^{21} V/m^2) with asymmetry parameter 0.54 is in excellent agreement with the measured value of V_{zz} extrapolated to 0 K ($7.3(2)\times10^{21}$ V/m^2) and η at 77 K (0.52(1)) for the component Zr_7Ni_{10}, thus confirming that the mentioned component of the measured PAC spectra originates from Zr_7Ni_{10}.

5 Conclusion

In Zr_7Ni_{10} sample, the phases Zr_2Ni_7, Zr_7Ni_{10} and Zr_8Ni_{21} are produced where Zr_2Ni_7 is found as a major phase and a minor phase due to Zr_8Ni_{21} is found at room temperature. In Zr_7Ni_{10}, four non-equivalent crystallographic sites of Zr have been found. Our experimental results of EFG (V_{zz}) and η are in excellent agreement with those calculated at ^{181}Ta sites corresponding to Zr3 position in Zr_7Ni_{10} by the first-principles density functional theory based on the full potential (linearized) augmented plane waves method [FP-(L)APW]. The origin of observed EFG in Zr_7Ni_{10} can thus be explained.

Acknowledgements The authors thankfully acknowledge Mr. A. Karmahapatra of Saha Institute of Nuclear Physics, Kolkata for X-ray diffraction measurements. The present work is supported by the Department of Atomic Energy, Government of India through the Grant no. 12-R&D-SIN-5.02-0102 and by The Ministry of Education, Science and Technological Department of the Republic of Serbia through the Grant no. 171001.

References

1. Joubert, J.-M., Latroche, M., Percheron-Guégan, A.: J. Alloys Compd. **231**, 494 (1995)
2. Ruiz, F.C., Castro, E.B., Real, S.G., Peretti, H.A., Visintin, A., Triaca, W.E.: Int. J. Hydrog. Energy **33**, 3576 (2008)
3. Nei, J., Young, K., Regmi, R., Lawes, G., Salley, S.O., Ng, K.Y.S.: Int. J. Hydrog. Energy **37**, 16042 (2012)
4. Young, K., Ouchi, T., Fetcenko, M.A., Mays, W., Reichman, B.: Int. J. Hydrog. Energy **34**, 8695 (2009)
5. Young, K.-H., Nei, J.: Materials **6**, 4574 (2013)
6. Ruiz, F.C., Castro, E.B., Peretti, H.A., Visintin, A.: Int. J. Hydrog. Energy **35**, 9879 (2010)
7. Young, K., Nei, J., Ouchi, T., Fetcenko, M.A.: J. Alloys Compd. **509**, 2277 (2011)
8. Kirkpatrick, M.E., Smith, J.F., Larsen, W.L.: Acta Crystallogr. **15**, 894 (1962)
9. Joubert, J.-M., Černý, R., Yvon, K., Latroche, M., Percheron-Guégan, A.: Acta Crystallogr., Sect. C: Cryst. Struct. Commun. **53**, 1536 (1997)
10. Schatz, G., Weidinger, A.: Nuclear condensed matter physics: nuclear methods and applications (1996)
11. Dey, S.K., Dey, C.C., Saha, S., Belošević-Čavor, J.: Intermetallics **84**, 112 (2017)
12. Dey, S.K., et al.: J. Solid State Chem. **269**, 476 (2019)
13. Béraud, R., Berkes, I., Daniére, J., Marest, G., Rougny, R.: Nucl. Inst. Methods **69**, 41 (1969)
14. Zacate, M., Jaeger, H.: Defect Diffus Forum **311**, 3 (2011)
15. Joubert, J.-M., Černý, R., Yvon, K., Krist, Z.: New Cryst. Struct. **213**, 227 (1998)
16. Eshelman, F.R., Smith, J.F.: Acta Crystallographica Section B **28**, 1594 (1972)
17. Rodríguez-Carvajal, J.: Phys. B Condens. Matter **192**, 55 (1993)
18. Dey, C.C., Srivastava, S.K.: Phys. B Condens. Matter **427**, 126 (2013)
19. Dai, C., Saidi, P., Yao, Z., Daymond, M.R.: Acta Mater. **140**, 56 (2017)
20. Nash, P., Jayanth, C.S.: Bull. Alloy Phase Diagr. **5**, 144 (1984)
21. Wodniecka, B., Marszałek, M., Wodniecki, P., Hrynkiewicz, A.Z.: Hyperfine Interact. **80**, 1039 (1993)
22. Wodniecki, P., Wodniecka, B., Kulińska, A., Uhrmacher, M., Lieb, K.P.: J. Alloys Compd. **312**, 17 (2000)
23. Wodniecka, B., et al.: J. Alloys Compd. **219**, 132 (1995). Eleventh international conference on solid compounds of transition elements
24. Wodniecki, P., Wodniecka, B., Marszałek, M., Hrynkiewicz, A.Z.: Zeitschrift für Naturforschung A **51**, 437 (1996)
25. Wodniecki, P., Wodniecka, B., Kulińska, A., Hrynkiewicz, A.Z.: Zeitschrift für Naturforschung A **53**, 355 (1998)
26. Wodniecki, P., Kulińska, A., Wodniecka, B., Hrynkiewicz, A.Z.: Zeitschrift für Naturforschung A **53**, 349 (1998)
27. Petrilli, H.M., Marszałek, M., Saitovitch, H.: Zeitschrift für Naturforschung A **51**, 537 (1996)
28. Blaha, P., Schwarz, K., Madsen, G.K.H., Kvasnicka, D., Luitz, J.: WIEN 2k: an augmented plane wave plus local orbitals program for calculating crystal properties, Vienna University of Technology, Vienna, Austria (2001)
29. Perdew, J.P., Burke, K., Ernzerhof, M.: Phys. Rev. Lett. **77**, 3865 (1996)
30. Perdew, J.P., Burke, K., Ernzerhof, M.: Phys. Rev. Lett. **78**, 1396 (1997)
31. Zhang, Y., Yang, W.: Phys. Rev. Lett. **80**, 890 (1998)
32. Belošević-Čavor, J., Koteski, V., Radaković, J.: Solid State Commun. **152**, 1072 (2012)
33. Blaha, P., Schwarz, K., Herzig, P.: Phys. Rev. Lett. **54**, 1192 (1985)